

# Silica laser damage mechanisms, precursors and their mitigation

J. Bude, P.E. Miller, N. Shen, T. Suratwala, T. Laurence, W. Steele, S. Baxamusa, L. Wong, W. Carr, D. Cross, M. Monticelli, M. Feit, G. Guss

Lawrence Livermore National Laboratory  
7000 East Avenue, L-460, Livermore, CA 94550 USA

## ABSTRACT

Controlling laser damage is essential for reliable and cost-effective operation of high energy laser systems. We will review important optical damage precursors in silica up to UV fluences as high as  $45\text{J}/\text{cm}^2$  (3ns) along with studies of the damage mechanisms involved and processes to mitigate damage precursors. We have found that silica surface damage is initiated by nano-scale precursor absorption followed by thermal coupling to the silica lattice and formation of a laser-supported absorption front. Residual polishing compound and defect layers on fracture surfaces are primarily responsible for optic damage below about  $10\text{J}/\text{cm}^2$ ; they can be mitigated by an optimized oxide etch processes. At fluences above about  $10\text{J}/\text{cm}^2$ , precipitates of trace impurities are responsible for damage; they can be mitigated by eliminating the chances of impurity precipitation following wet chemical processing. Using these approaches, silica damage densities can be reduced by many orders of magnitude allowing large increases in the maximum operating fluences these optics see.

**Keywords:** laser damage, damage mechanisms, laser matter interactions, fused silica optics, glass optics, optics processing, damage resistant optics, laser damage testing

## 1. INTRODUCTION

High energy laser systems such as the National Ignition Facility (NIF) [1] typically need to operate beyond the laser damage threshold of important optics in order to meet their full mission needs in areas including high energy density science and inertial confinement fusion (ICF) [2]. This is particularly true of UV optics such as the conversion crystals and the fused silica focusing optics used in final optics assemblies where surface laser damage ultimately limits performance [3]. Hence there is a need for focused efforts aimed at the reduction and mitigation of surface damage in order to achieve cost effective operation of these systems at desired fluence levels. This is particularly important for silica optics since initiated surface damage in silica grows rapidly with shot number [4].

Figure 1 shows a plot of the improvement of silica surface damage initiation density for NIF optics ( $1100\text{cm}^2$ ) as a function of 355nm fluence with 3ns Gaussian pulses from the late 1990's to the present. Each generation has seen a reduction in the overall damage density,  $\rho(\phi)$ , and an increase in damage threshold as defined by the fluence onset of measureable damage (one site per optic). The damage density for these optics has been plotted together with a fluence histogram for a typical 1.8MJ 500TW ICF-type ignition pulse [2]. Optics produced in 1997 would have been expected to have tens of thousands of damage initiations for these shots. By 2007 improvements in finishing quality [5] reduced the number of damage initiations to hundreds of sites, and as seen in the plot, significant improvements have continued to the present day.. This paper discusses research advances which have driven these improvements. in particular, an understanding of silica damage mechanisms and the properties of damage precursors (the absorbers which lead to optical damage), an identification of the most important damage precursors in a given fluence range, and the means to reduce or eliminate these precursors (mitigation). This work has led to the Advanced Mitigation Processes (AMP) shown in Figure 1, referred to as the AMP2 [6] and AMP3 [7] generations of AMP, which push damage densities toward zero for reasonable fluence ranges (below  $45\text{J}/\text{cm}^2$ ).

The articles referred to below discuss these advances but our list is by no means complete; please see the additional references cited in these works for more complete background and detail. Also, with respect to laser damage testing: all damage testing described below was obtained at 355nm with either 3ns Gaussian (GS) pulses or 5ns flat-in-time (FIT) pulses. It has been found from pulse-length scaling studies that these are equivalent from a damage perspective [8]. Laser damage testing was performed with small beam and large beam protocols: for R/1 small beam testing protocols see [9]; small beam S/1 arrays were used to estimate damage density up to 160J/cm<sup>2</sup> [10]; and, large beam damage testing was performed in the Optical Sciences Laboratory (OSL) using 1 and 3cm<sup>2</sup> beams with 5ns FIT pulses [11].

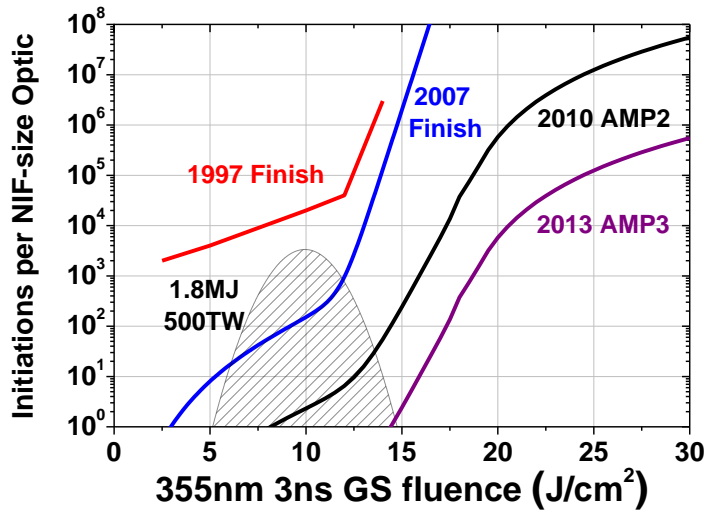


Figure 1: NIF silica optic surface damage density improvement from 1997 to the present: damage initiations per NIF-sized optic (1100cm<sup>2</sup>) at 355nm with 3ns Gaussian (GS) pulses. A fluence histogram for a typical ICF shot [2] is shown along with the damage density

## 2. Silica damage mechanisms and precursors

Identifying surface damage precursors is challenging since typical methods of surface characterization are not reliable diagnostics for damage: there are many surface features found by optical microscopy which don't damage and damage often occurs in regions of an optic having no observable features. Understanding the mechanisms of silica surface damage helps to define what properties a damage precursor must have to create a damage site which grows upon exposure to multiple laser pulses, and thus, serves as a guide to looking for precursors. Tested models for laser damage can also clarify the physics for damage initiation and growth as a function of laser parameters such as fluence and pulse shape.

Figure 2a shows a typical silica surface damage site upon initiation with a single laser pulse. Sites can initiate with sizes from 5um to 30um depending on the pulse shape, but all sites which subsequently grow have a molten central region surrounded by a fracture network suggestive of explosive ejection of material from below the surface. Often these micron-scale damage sites are generated from absorbers too small to see optically – nano-scale absorbers. Hence, surface damage requires that an absorbing defect couple laser energy into the near-surface bulk glass. One model which describes this process well is the absorption-front (AF) model [12]. The process begins when a near surface precursor is heated by the absorption of laser light (sub band-gap with respect to the bulk). When the material around this precursor reaches a sufficient temperature, the bulk (intrinsic) glass begins to absorb light through temperature-activated intrinsic absorption with an absorption coefficient  $\alpha_{INT}(T)$ . Intrinsic absorption leads to a thermal run-away driving the glass temperature as high as 10,000K as more laser energy is coupled into the heated glass. This process can continue until the end of the laser pulse. *The coupling of thermal conduction with T-activated absorption provides the mechanism by which this energy spreads into the bulk back towards the laser with a nearly constant velocity – a laser-supported absorption front.* AF propagation velocities are much higher than energy transport via diffusion alone could provide. This behavior is driven by temperature activated absorption plus thermal conduction by both phonons and thermally activated free

carriers. In fact, thermally activated thermal conduction by free carriers is necessary to describe the observed behavior [12]. Figure 2b shows a hydrodynamic simulation of an absorption front propagating away from an absorbing precursor back towards the laser source. The AF leaves a region of super-heated material microns below and around the original absorber, and explosive ejection of this material leads to the molten core and fracture region seen in Figure 2a.

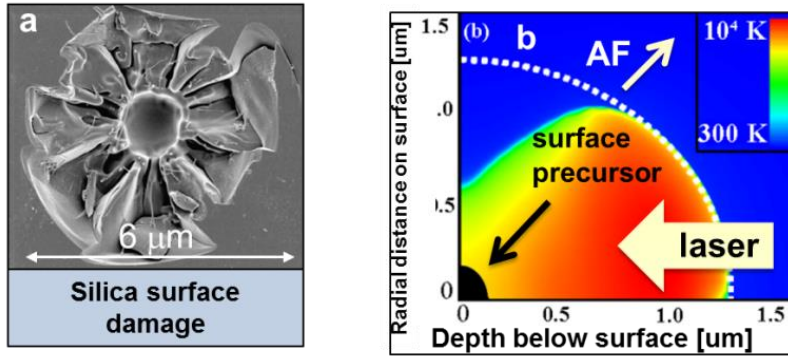


Figure 2: (a) Laser initiated silica surface damage site. Sites such as these with fracture networks grow upon future exposure to laser light and limit an optics lifetime. (b) Hydro-dynamic simulation of laser supported absorption front (AF) formation from a surface nano-scale damage precursor (see [12]).

**Precursor absorptivity:** An essential feature of this model is the demonstration of temperature activated intrinsic absorption. Direct measurements of the temperature dependence of optical absorption are limited to temperatures below the melting point and to high energy photons near the band-edge of silica [13]. We have used indirect methods to estimate T-activated absorption at 355nm (far below the band-edge) and to demonstrate the role of temperature activated absorption in surface damage. Such experiments use a pulsed mid-IR laser (10.6μm) to heat the silica surface to temperatures well above the melting point, and a 355nm ns laser is focused through the heated region and triggered at the end of the heating pulse (see for example [14]). The interaction of the 355nm pulsed laser with the heated glass leads to material removal and damage consistent with temperature activated absorption -- damage happens at lower fluences on surfaces that have been heated. The fluence dependence of the damage combined with in-situ temperature diagnostics and simulations of thermal run-away yield estimates for  $\alpha_{INT}(T)$  shown by the symbols in Figure 3.

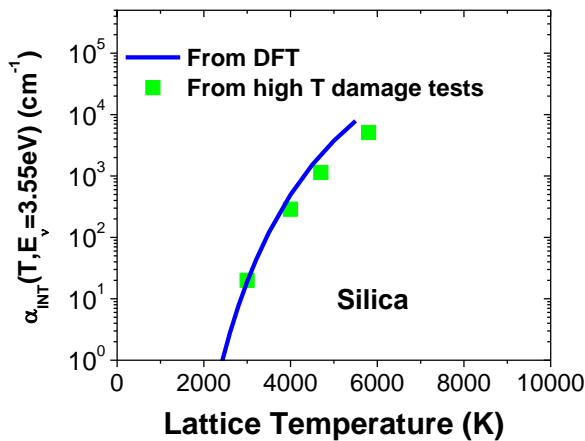


Figure 3: Intrinsic absorption coefficient in silica,  $\alpha_{INT}$ , at 355nm as a function of temperature as estimated from high temperature damage threshold measurements and computed by ab-initio DFT simulations.

We also performed time dependent ab-initio density functional theory (DFT) simulations to estimate  $\alpha_{INT}(T)$  [14]. These simulations agree well with the direct measurements of absorptivity performed at lower temperatures [13] and provide values at 355nm (3.5eV) for the temperature range shown in Figure 3. Simulated results are plotted together with the

high temperature damage data in Figure 3 showing excellent agreement. Analysis of the DFT simulations indicate that temperature-activated absorption in silica is due to the Urbach broadening of the band edge, band-gap narrowing and at 10,000K, band-gap collapse. These processes are the result of thermal-induced disorder of the atomic structure of silica at high temperatures which creates band-tail states and a reduction of the band-gap. Based on these values for  $\alpha_{INT}(T)$ , thermal run-away will occur when the temperature of a suitable precursor reaches 3,000 to 4,000K. Therefore damage precursors must absorb enough light to during the laser pulse to reach these temperatures. Hence, in silica, thermal run-away and AF formation is not related to phase transformations such as heating to the melting point of the material, but is driven by Urbach processes. This typically requires that the precursor have an absorptivity of greater than  $10^4 \text{ cm}^{-1}$  depending on precursor size. Energy transport models were developed to include these effects. The model has been validated for both model systems [16] and in surface damage experiments [12].

**Surface adhesion and thermal coupling:** The experimental demonstration on model systems highlighted another important property of surface damage precursors – surface adhesion. In these experiments, Al pillars were patterned on a silica surface, furnace annealed at temperatures between 500°C and 600°C, and exposed to laser light [16]. Given the known absorptivity of Al, a simple 1D heat transport model was used to compute the Al temperature as a function of laser fluence. This work showed a clear threshold above which fractured damage sites were formed and below which the Al was removed without substrate damage (Figure 4a). Simulations showed that this threshold corresponds to the onset of thermal run-away via the AF model (Figure 4b). The higher the fluence, the deeper the AF penetrated and the deeper the resulting damage pit (and the greater the fracture). The furnace anneal was necessary to ensure sufficient adhesion to the surface. Without it, the Al films escape from the surface before enough heat flows into the substrate to initiate an AF. Although the un-annealed Al films became very hot (many thousands of K), the substrate sees only modest (100nm) surface perturbation. Hence a damage precursor may be nano-scale, but it must absorb enough light to launch an AF and it must be strongly (chemically and vibronically) bonded to the surface or in fact, to be defects in the silica itself. Adhesion to the surface and thermal coupling is important for particle and contaminant-related damage as well.

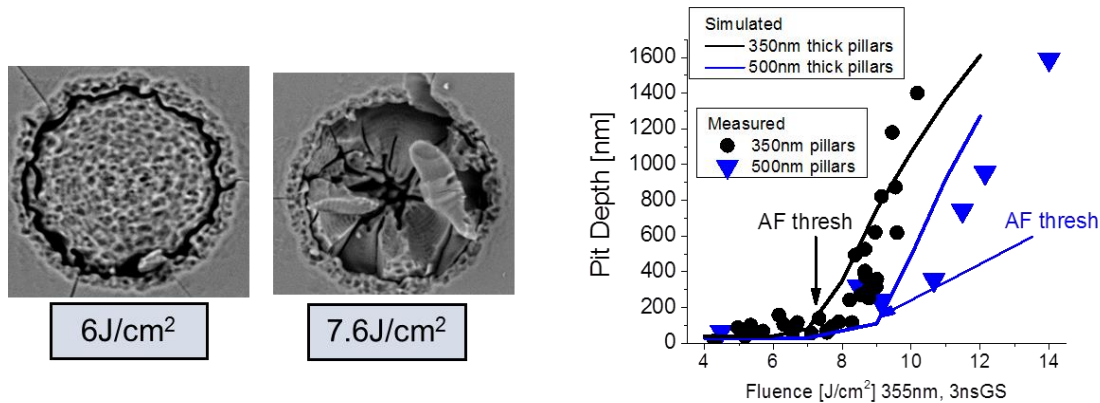


Figure 4: Experimental demonstration of AF formation and damage in silica [16]. Figure 4a (left): micrographs of Al pillars on silica surfaces after exposure to 355nm laser pulses – 6J/cm<sup>2</sup>, below AF threshold, 7.6J/cm<sup>2</sup>, above AF threshold, damage site with fracture. Figure 4b (right): simulated and measured pit depths created by AFs showing threshold conditions (temperature) for absorption front formation.

### 3. Fracture surface defect layers as primary damage precursors below 10J/cm<sup>2</sup>

Damage precursors strongly absorb sub band-gap light, effectively transfer that energy to the silica glass matrix, and can be sub-100nm in size. In this section we will address the damage precursors which contribute to the damage shown in Figure 1 below 10J/cm<sup>2</sup> and which were responsible for many hundreds of damage sites for the optics such as those from circa 2007 when exposed to a 1.8MJ ICF laser shot (see Fig. 1). Here, we look at precursors on silica surfaces free of particulates and gross contamination. Such sources of contamination are known to damage optics in general [17], and can be mitigated using standard cleanliness protocols prior to use in a laser system; contamination during laser operation

must also be addressed. The improvements in surface quality from the 1990's surface finish to surface finishes typically available in 2007 were the result of a significant reduction in polishing related surface damage [5], so it is natural to begin looking for damage precursors related to surface damage.

The processes involved in material removal during polishing introduce mechanical and chemical modifications to the silica surface which may be associated with laser damage. These include contamination from residual polishing compounds (typically Ce or Fe in MRF systems), structural densification of the glass, plastic deformation and fracture. Ce and Fe contamination will result in laser damage, but can be removed by acid leaching or weak etching chemistry [18]. However, structural flaws and the precursors primarily responsible for damage below  $10\text{J}/\text{cm}^2$  remain. To address these precursors and propose mitigation strategies, we performed a controlled indentation study to understand what aspect of a flaw leads to laser damage. Various candidates include optical field intensification due to fractures, impurities trapped in fractures and defects associated with plastic deformation, structural densification or the fracture itself (Figure 5). Here, we briefly describe results from this study (see [19] for complete details).

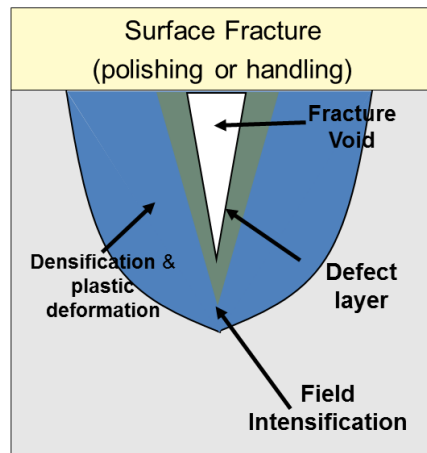


Figure 5: Potential damage precursors associated with surface flaws created by polishing and handling.

This study used static indentation to produce, in a controlled way, structural modifications associated with finishing. A variety of micro-indenters were used including diamond shaped Vickers, and Knoop indenters as well as a ball-type (blunt) Brinell's indenter. Various loads were applied, and the resulting surface perturbations were studied with a variety of techniques including optical, and secondary electron microscopy, time-resolved confocal photoluminescence imaging [20] and laser damage testing. Figure 6 shows a 0.5N Vickers indentation on a silica surface. At this load, the material beneath the indent is densified, but no noticeable fracture is visible optically. Photoluminescence images (Figure 6b) show a strongly photo-active species lining the periphery of the indent. The photoluminescence was broadband and exhibited a broad continuum of lifetimes down into the pico-second regime. This type of quasi-continuum (QC) photoluminescence is associated with a high density of interacting defects [20] and has been correlated to laser damage. From the discussion above, it is clear that laser damage precursors must have a very high absorptivity ( $> 10^4 \text{ cm}^{-1}$  at 355nm) in order to reach temperatures sufficient to result in thermal run-away and AF formation; it is expected that the high density of interacting defects associated with QC photoluminescence could provide such a strong absorption.

Initially it was unclear what structural feature was associated with this ring of photoluminescence. The densified material exists throughout the entire area of the indent, but the QC PL was found only on the edge. We would expect that the material at the edge was modified by plastic deformation, but separate experiments in [19] ruled this out as well. Careful examination of this indent with SEM showed very fine fractures ( $< 20\text{nm}$ ) on the periphery of each indentation. . These subtle fractures were correlated with the PL and hence were strongly photo-active. Laser damage testing confirmed that damage occurred first on these fracture cusps as well. Studies of larger indents such as the 10N Vicker's indent in Figure 7 clearly show that these damage precursors are confined to within 500nm of the fracture surface (see for example, the confocal PL image of a cross sectional plane through the surface of the 10N indent in Figure 7B).

Further experiments on shallow fractures, that were subsequently etched in aqueous hydrofluoric acid solutions showed that the defect layer is even thinner, lying within 100nm of the fracture surface. For larger fractures, optical field intensification could potentially play a role as well. However, work with the deeper etches discussed below make this unlikely. In addition recent laser conditioning experiments prove this as it is possible to increase damage thresholds of such fractures by pulsed ns-laser conditioning which produces no structural modification of the fracture [21]. Hence, we conclude that very thin (nano-scale thick) defect layers along fracture surfaces are the main source of damage precursors and damage associated with surface flaws.

### 0.5N Vicker's Indentations

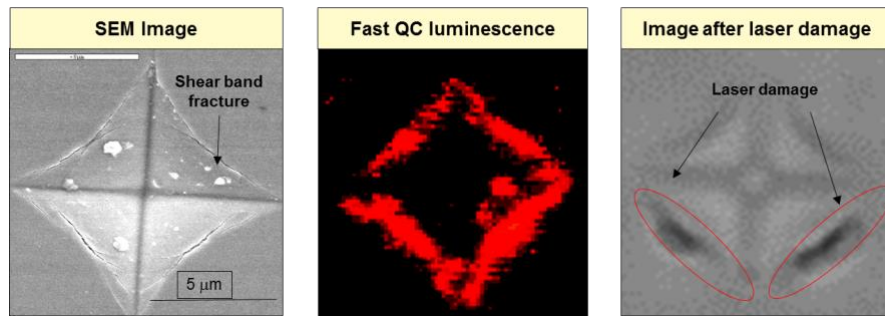


Figure 6: Low load 0.5N indent on silica surface: SEM image showing 20nm wide surface fractures; QC PL surface image showing correlation of highly absorbing species with fine fractures; microscope image after laser exposure showing correlation between damage, PL and fracture [19].

### 10N Vicker's Indentations

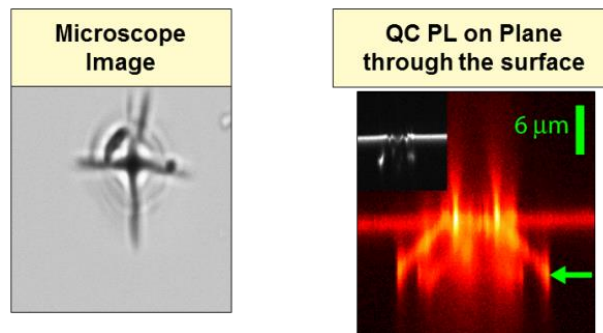


Figure 7: High load 10N Vicker's indent with extensive fracture: microscope image and confocal time-resolved QC PL image through the fracture showing photo-active species on the fracture surfaces [19].

Identification of fracture surfaces as damage precursors suggests an etch-based mitigation. We used an HF acid-based etch to open surface fractures and remove the absorbing defect layer [6]. A shallow etch (100nm) of the 0.5N indent in Figure 6 completely removed the PL and increased the damage threshold to a value consistent with that observed on a fracture free portion of the surface [19]. Longer etches were needed to fully etch deeper fractures. Initial studies for deep fracture etching actually decreased the laser damage threshold. Examination of these deeper etches revealed the presence of etch-product precipitates; such precipitates were found to be photo-active as observed by PL imaging and easily damaged upon laser exposure. It is likely that earlier attempts to increase silica damage thresholds by oxide etches were affected by these etch products; in fact, etch products can actually reduce the surface damage threshold.

In view of these results, we conducted a series of etch studies designed to remove the fracture-defect layer without leaving damage limiting etch-precipitates (see [6] for full details of this study). Such a process is briefly described below. For these studies, we created a series of surface fractures by sliding silica spheres along an optic's surface. The

samples were then cleaned and the width of the fractures were measured. The samples were then treated with various etch recipes, laser damage tested, and damage thresholds as a function of scratch width were recorded. The depth of a scratch's sub-surface fracture is related to its width; deep scratches required longer etch times to ensure that the fracture was fully opened and the defect layer removed. As a consequence, for a given etch, the damage threshold of the wider (deeper) scratches was lower.

Some of the etch conditions that were chosen to reduce formation of precipitates in the opened fractures are described below. For instance, we found that ultra-sonic agitation during etching facilitates more effective removal of the etch products, and damage thresholds were increased under these conditions. The chemistry of the buffered oxide etch (BOE) was also modified to reduce the concentration of the  $\text{NH}_4^+$  based fluoride buffering agent. Reduction of concentration of  $\text{NH}_4^+$  increases the solubility of the corresponding hexafluorosilicate salt thus reducing the potential for precipitation of etch byproducts on the glass surfaces. The etch depth and the specific details of the rinse process were similarly optimized to ensure that the widest fractures were mitigated. A particularly important aspect of these studies was the need to ensure adequate mass transport of etch products from the opened fractures. We found that in an optimized process, a 20um etch was sufficient to fully mitigate scratches up to 50um wide (those commonly found on optics). This process was implemented in the NIF large optics production facility as the Advanced Mitigation Process, AMP2. AMP2 increases the damage threshold of scratches from as low as  $5\text{J}/\text{cm}^2$  to values above  $15\text{J}/\text{cm}^2$ . AMP2 has been quite successful (see Figure 1): to date, we have found essentially no scratch related damage initiations on AMP2 treated optics fielded on NIF; such optics have seen thousands of shots up to fluences of  $10\text{J}/\text{cm}^2$ .

#### 4. Nano-scale precipitates from processing as damage precursors above $10\text{J}/\text{cm}^2$

While the AMP2 process fully mitigates fracture-related damage and significantly reduces damage density for fluences below  $10\text{J}/\text{cm}^2$ , there remain classes of precursors which lead to a sharp rise in damage initiations above  $10\text{J}/\text{cm}^2$ . These "high fluence" precursors are not associated with any readily observable feature on the surface (such as surface flaws or roughness) and are too subtle to be detected by photo-luminescence or photo-thermal imaging. This threshold-like behavior is seen in many materials and sometimes suggests an intrinsic damage threshold associated with intrinsic material or surface property. However, measurements of the damage density out to  $160\text{J}/\text{cm}^2$  suggest an extrinsic mechanism with most of the damage precursors lying below  $40\text{J}/\text{cm}^2$  for 3ns Gaussian pulses [10] (see Figure 8). Above about  $40\text{J}/\text{cm}^2$  the damage density becomes fairly flat indicating a nearly constant precursor density. In fact, small beam damage tests demonstrate that there are significant fractions of the surface that are free of damage precursors when exposed to fluences of to  $160\text{J}/\text{cm}^2$  (see Figure 8).

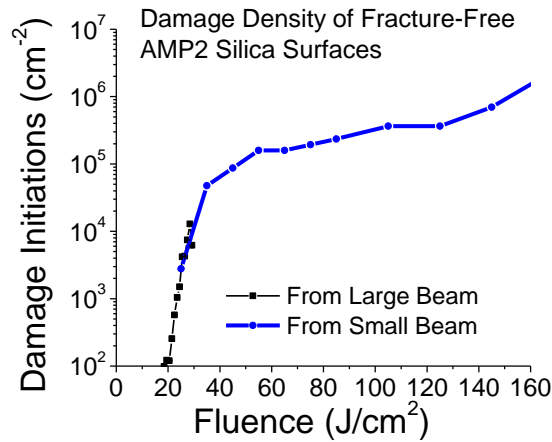


Figure 8: Damage density measured on an AMP2 surface as a function of 355nm fluence out to  $160\text{J}/\text{cm}^2$ . Measurements are a compilation of large beam damage tests at lower fluences and small beam S/1 tests performed as per [10].

Identification of precursors in this fluence region was problematic, because unlike the lower fluence precursors where we could make model flaws (indentations) and study their properties and isolate the damage-causing feature, there was no known way to create model high fluence precursors. AMP2 processed optics always had them. Hence, we looked to laser-based methods to create damage-free regions of the surface. The goal was to see if we could determine which surface changes led to reduced damage and whether or how re-processing would introduce new precursors. The method we adopted is based on mid-IR based damage site mitigation protocols [22] which use local surface heating to increase the surface damage threshold [22,15]. This process uses pulses from a 10.6um CO<sub>2</sub> laser to heat a several mm region on the surface beyond 2,000K for periods of time up to a second. Results of such a process are shown in Figure 9A which plots the small beam R/1 damage threshold as a function of position through a 2mm wide heated region of the surface. The damage thresholds shown in this Figure are quoted relative to the AMP2 surface threshold. Here, the R/1 threshold of the heated region was more than 60% higher than the un-heated surface. Characterization of this region showed a number of changes to the surface which could have been responsible for the increased damage threshold: surface smoothing (down to Angstroms), de-hydration of the glass below the surface (reduced OH content), densification of the glass upon cooling and surface evaporation removing about 100nm of material. Unfortunately, it was not possible to link any one of these to reduced damage because none could be decoupled from the other. Such sites however proved to be ideal for re-processing studies.

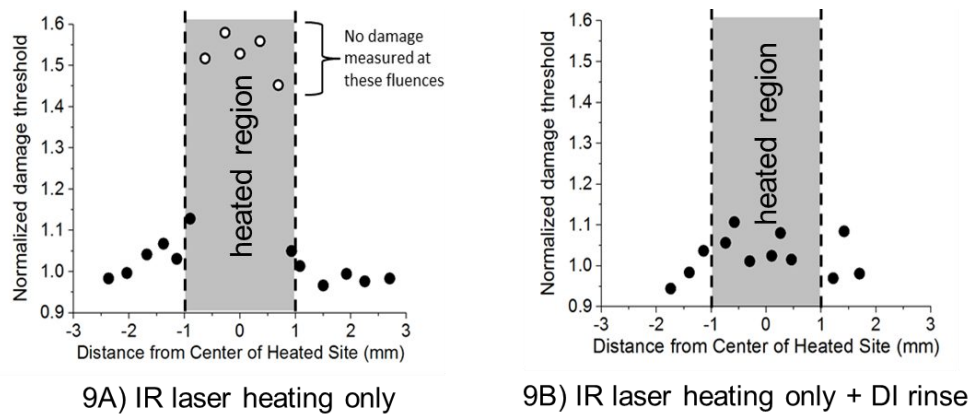


Figure 9: Damage thresholds measured as a line-out through 2mm regions of an AMP2 silica surface heating by a CO<sub>2</sub> laser to temperatures greater than 2,000K. Figure 9A (left): S/1 thresholds measured after CO<sub>2</sub> laser heating. Figure 9B (right): S/1 thresholds measured after DI water rinse of samples in 9A [7].

To this end, we created a series of mid-IR laser heated sites on a set of AMP2 silica substrates. R/1 damage thresholds were measured on controls for each sample to ensure efficacy of the heat treatment. Then, samples were passed through the various steps in the AMP2 process working backwards from the last step to the first; steps tested included surface drag wiping, a de-ionized (DI) water spray rinse, an ultra-sonic DI water rinse bath, and mega-sonic BOE etching. The strategy was to see whether any of these steps re-introduced high fluence precursors. In fact, the results demonstrated that all of the wet processing steps did. Figure 9B shows results of a heat-treated site like that in Figure 9A after a DI spray rinse. The damage threshold of the entire site returned to values near that of the rest of the surface, *so that reprocessing, even with DI water, leaves damage precursors linked to high fluence damage* [7]. These results implicate either water-silica surface chemistry or trace contaminants carried in the water.

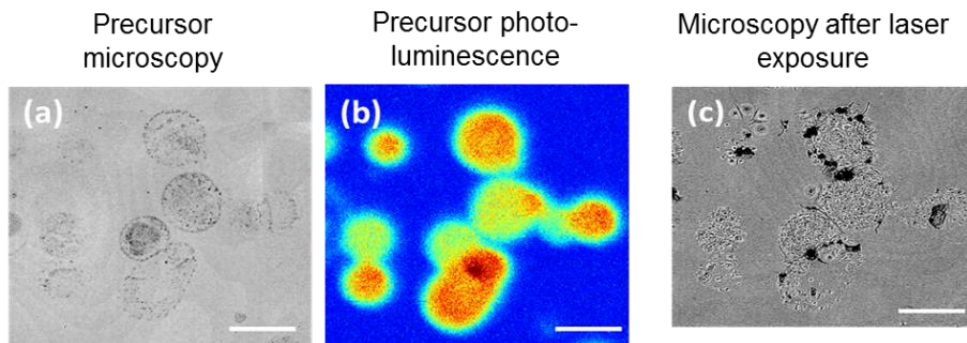


Figure 10: Demonstration that precipitates of NaCl salts on silica surfaces are laser damage precursors at 355nm [7].

Even 18M $\Omega$ -cm deionized water often has part per billion quantities of dissolved ionic impurities; the most common are simple sodium ( $\text{Na}^+$ ), calcium ( $\text{Ca}^{2+}$ ) or potassium ( $\text{K}^+$ ) based salts. If such salts form high fluence precursors, their precipitates should be nano-scale (hence invisible to optical microscopy); and, based on the discussion in Section 2, they must absorb strongly in the UV (reaching thermal run-away during the laser pulse), and they should be bonded firmly to the surface. As impurity loads in our processing liquids are very low and precursor densities are high -- more than  $10^5 \text{ cm}^{-2}$  (see Figure 8) -- it is reasonable to expect that precipitates would be small, possibly nano-scale. It is also likely that impurities deposited during drying on silica surfaces would be reasonably adherent (compared to, for instance, contaminants introduced onto a dry optic). It was, however, unclear whether precipitated salts could absorb sufficient UV light to initiate laser damage. To test whether precipitates of common salts could initiate damage, we prepared a solution of NaCl and applied it to silica surfaces as aerosolized mist. Because the NaCl concentration was high, the precipitates which formed were large (many microns) and were readily visible by optical microscopy (Figure 10a). Photoluminescence images clearly demonstrated that such precipitated salts were photo-active (10b). Laser damage testing revealed that such precipitates did initiate laser damage (10c). In fact, R/1 tests of a variety of common salts and the organic solute sucrose all led to laser damage as seen in Figure 11. Here, the control is the uncontaminated AMP2 silica surface. Figure 11 also shows the bulk band-gap of these salts, all of which are much higher than the photon energy of 3.55eV (355nm), so that the optical absorption in the bulk of these materials cannot lead to damage. Therefore, the absorption which leads to laser damage likely occurs on defective surfaces in some way similar to the fracture defect layers. *Many precipitates absorb enough energy to be laser damage precursors, even if the bulk material is nominally transparent. The optical absorption which leads to damage must occur on defects associated with heterogeneous precipitation on silica surfaces.*

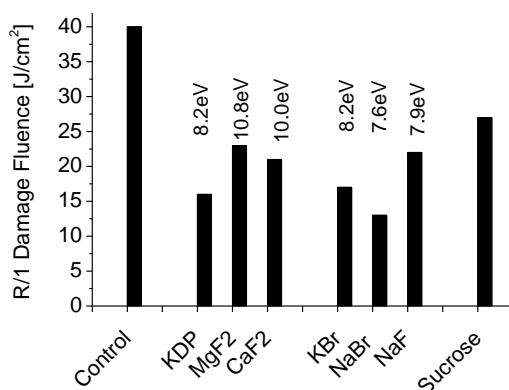


Figure 11: R/1 laser damage thresholds for materials precipitated on silica surfaces – this demonstrates that precipitates of common salts and the organic solute sucrose can be surface damage precursors. The control sample corresponds to the uncontaminated silica surface. The band-gap energies for the bulk materials show that they are nominally transparent to 355nm light.

To prove that precipitates from wet chemical processing were *the limiting high fluence precursors remaining in the AMP2 process*, we investigated whether we could reduce damage densities through processes designed to suppress impurity precipitation. These process improvements concentrated on the wet chemical processing steps including etching, rinsing and drying (see full description in [7]). Steps included careful control of impurity levels in the reagents and in the quality of the DI water, reduction of airborne particles which could contaminate processing liquids or on drying surfaces (all samples were processed in a Class 100 cleanroom), reduction of contaminants in all lab-ware, in fixuring, and controlled drying to ensure uniform thin liquid films with no concentration of liquids on the surface (for example, droplets).

A survey of these samples clearly showed a correlation between nano-scale precipitates as measured by atomic force microscopy (AFM) and laser damage. AFM studies of these samples revealed that after drying, nodule-like features appear on this otherwise smooth surface; they have typical dimensions less than 100nm in the plane and tens of nm high. Figure 12 plots the AFM nodule count density versus the damage density computed from laser damage tests using a 1cm<sup>2</sup>, 5ns FIT (3ns GS), 355nm laser beam. Damage density is plotted in cm<sup>-2</sup> at 40J/cm<sup>2</sup>. A correlation is shown in which the nodule density tracks the damage density. Note that nodule density is always somewhat higher than damage density as it should be -- some of these nodules probably don't damage at test fluences. We interpret these nodules as process-related precipitates which are visible when surfaces are clean and smooth enough to get good AFM data.

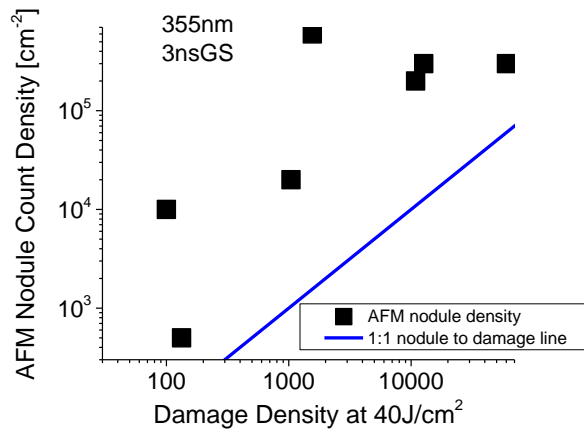


Figure 12: Correlation between AFM nodule counts and damage density at 40J/cm<sup>2</sup> for a survey of AMP processed samples [7].

We estimated the impact of various impurity concentration on damage performance for different parts of the AMP process. One such result is shown in Figure 13. We designed this study to look at the effects of DI water purity on damage density measured as above at 40J/cm<sup>2</sup> in order to prove that the impurities *found in our DI water* would produce high fluence precursors. To this end, we started with 18MOhm-cm DI water (the measurement limit of ionic impurities set by the auto-disassociation of water), and doped such solution with untreated municipal water; the resulting mixture then mimics varying levels of de-ionization of the input water stream. Two experiments are shown: one in which the contaminated water was introduced in the AMP2 etch bath, and one in which it was introduced into the final DI water spray rinse. All other parts of the process were left un-touched. The result shows that impure DI water in either source increases damage density, but that the effect is much stronger when the impure water is introduced into the final rinse. It is likely that impurities in the etch bath near the beginning of the process are in some part removed during subsequent processing, whereas impurities in the final rinse will necessarily dry on the optic's surface. Experiments like this lead to the conclusion that *high fluence damage increases strongly when processing impurity concentrations exceed 10ppb [AMP3 ref]*.

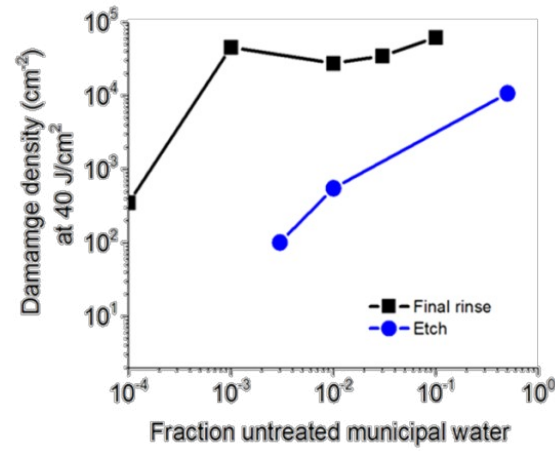


Figure 13: Plot of damage density at  $40\text{J}/\text{cm}^2$  as a function of untreated processing water introduced in both the etch step and the final optic rinse [7].

The AMP protocols developed here comprise the AMP3 process as shown in Figure 14. The damage density for AMP2 and AMP3 was measured using large beam damage tests in OSL. For fluences above about  $30\text{J}/\text{cm}^2$ , tests were performed with a  $1\text{cm}^2$  beam; multiple samples were averaged. In order to accurately measure the low AMP3 damage density below  $30\text{J}/\text{cm}^2$ , we also performed tests with an average fluence of  $23\text{J}/\text{cm}^2$  (with tails up to  $32\text{J}/\text{cm}^2$ ), and at an average fluence of  $15\text{J}/\text{cm}^2$  (with tails up to  $25\text{J}/\text{cm}^2$ ) over about  $32\text{cm}^2$  of tested area. The test at  $23\text{J}/\text{cm}^2$  yielded one damage site, and the test at  $15\text{J}/\text{cm}^2$  yielded no sites over  $32\text{cm}^2$ . The curve shown in Figure 14 is a best fit to all three of these measurements. Process modifications responsible for AMP3 reduced the damage density at high fluence ( $30\text{J}/\text{cm}^2$ ) by a factor of 300 compared to the AMP2 process and shifted the entire curve towards higher fluences by  $\approx 7\text{J}/\text{cm}^2$ . The AMP3 process is stable, consistently producing results like those shown here. This improvement would enable a 70% increase in silica optic operating fluence and a dramatic reduction in damage initiations at current operating points. More recent results [B] allow one to extend these improvements to 2000X reductions in damage density with a nearly  $10\text{J}/\text{cm}^2$  shift to higher fluence.

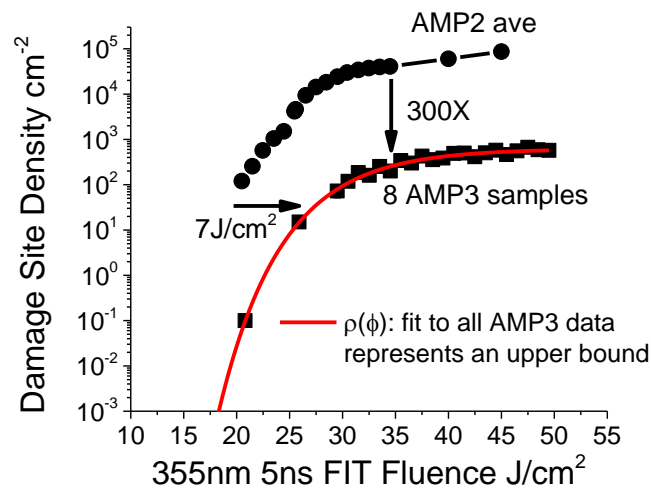


Figure 14: comparison of damage density between AMP2 and the AMP3 process optimized to reduce the probability of precipitation from wet chemical processes: shows a 300X reduction in overall damage density and a  $7\text{J}/\text{cm}^2$  shift to higher fluences [7].

## 5. Conclusions

Management and mitigation of silica laser damage is essential to ensure high performance and cost effective operation of high energy lasers such as the NIF. The work described above represents a focused long-term effort to understand and control laser damage on the surfaces of fused silica optics. Silica surface damage is initiated by nano-scale precursor absorption followed by thermal coupling to the silica lattice and formation of a laser-supported absorption front. Defect layers on fracture surfaces are primarily responsible for optic damage below about  $10\text{J}/\text{cm}^2$ ; they can be mitigated by an optimized oxide etch processes such as AMP2. At fluences above about  $10\text{J}/\text{cm}^2$ , precipitation of trace impurities following aqueous processing becomes the dominant source of damage precursors. Such precursors can be mitigated by minimizing the chance of impurity precipitation following wet chemical processing. Progress has been significant. Full implementation of the AMP3 process for large optics should result in essentially no silica surface damage for the 1.8MJ 500TW ignition shot shown in Figure 1. Work continues at the NIF to achieve these levels for large optics and to ensure that extraneous damage sources on-line are reduced so that the full potential of AMP3 can be realized.

## ACKNOWLEDGEMENTS

The authors wish to acknowledge the staff of LLNL's NIF Optics Processing Facilities for help with sample preparation and the Optical Sciences Laboratory who performed essential large-beam laser tests. This work was performed under the auspices of the U.S. Department of Energy by Lawrence Livermore National Laboratory under contract DE-AC52-07NA27344 within the LDRD program. LLNL-PROC-662783

## REFERENCES

1. C. A. Haynam, P. J. Wegner, J. M. Auerbach, M. W. Bowers, S. N. Dixit, G. V. Erbert, G. M. Heestand, M. A. Henesian, M. R. Hermann, K. S. Jancaitis, K. R. Manes, C. D. Marshall, N. C. Mehta, J. Menapace, E. Moses, J. R. Murray, M. C. Nostrand, C. D. Orth, R. Patterson, R. A. Sacks, M. J. Shaw, M. Spaeth, S. B. Sutton, W. H. Williams, C. C. Widmayer, R. K. White, S. T. Yang, and B. M. Van Wonerghem, "National Ignition Facility laser performance status," *Applied Optics* **46**, 3276-3303 (2007).
2. J. L. Kline, D. A. Callahan, S. H. Glenzer, N. B. Meezan, J. D. Moody et al. , "Holhram energetic scaling to 520 TW on the National Ignition Facility," *Phy. Plasmas*, **20**, 056314, 2013.
3. J. Folta, M. Nostrand, J. Honig, N. Wong, F. Ravizza, P. Geraghty, et al, "Mitigation of laser damage on National Ignition Facility Optics in Volume Production", *SPIE* vol. 8885, 88850Z-1 (2013).
4. M. A. Norton, E. E. Donohue, M. D. Feit, R. P. Hackel, W. G. Hollingsworth, A. M. Rubenchik, and M. L. Spaeth, "Growth of laser damage on the input surface of SiO<sub>2</sub> at 351 nm," *Proceedings of the SPIE - The International Society for Optical Engineering* **6403**, 64030L (2006).
5. T. Suratwala, L. Wong, P. Miller, M. Feit, J. Menapace, R. Steele, P. Davis, D. Walmer, "Sub-surface mechanical damage distributions during grinding of fused silica optics, *J. Non-Cryst. Solids*, **352**, 5601-17, 2006).
6. T. I. Suratwala, P. E. Miller, J. D. Bude, W. A. Steele, N. Shen, M. V. Monticelli, M. D. Feit, T. A. Laurence, M. A. Norton, C. W. Carr, and L. L. Wong, "HF-Based Etching Processes for Improving Laser Damage Resistance of Fused Silica Optical Surfaces," *Journal of the American Ceramic Society* **94**, 416-428 (2011).
7. J. Bude, P. Miller, S. Baxamusa, N. Shen, T. Laurence, W. Steele, T. Suratwala, L. Wong, W. Carr, D. Cross and M. Monticelli, "High fluence laser damage precursors and their mitigation in fused silica," *Opt. Exp.* Vol. **22**, 5839 (2014).
8. C. W. Carr, J. B. Trenholme, and M. L. Spaeth, "Effect of temporal pulse shape on optical damage," *Applied Physics Letters* **90**, 041110 (2007).
9. N. Shen, P. E. Miller, J. D. Bude, T. A. Laurence, T. I. Suratwala, W. A. Steele, M. D. Feit, and L. L. Wong, "Thermal annealing of laser damage precursors on fused silica surfaces," *Optical Engineering* **51**, 121817 (2012).
10. T. A. Laurence, J. D. Bude, S. Ly, N. Shen, and M. D. Feit, "Extracting the distribution of laser damage precursors on fused silica surfaces for 351 nm, 3 ns laser pulses at high fluences ( $20\text{-}150\text{ J}/\text{cm}^2$ )," *Optics Express* **20**, 11561-11573 (2012).
11. C. W. Carr, M. D. Feit, M. C. Nostrand, and J. J. Adams, "Techniques for qualitative and quantitative measurement of aspects of laser-induced damage important for laser beam propagation," *Measurement Science & Technology* **17**, 1958-1962 (2006).
12. C. W. Carr, J. D. Bude, and P. DeMange, "Laser-supported solid-state absorption fronts in silica," *Physical Review B* **82**, 184304 (2010).
13. K. Saito and A.J. Ikushima, *Physical Review B* **62**, 8584 (2000).
14. B. Sadigh, P. Erhart, D. Aberg, A. Trave, E. Schwegler, J. Bude, "First-Principles calculations of the Urbach Tail in the Optical Absorption Spectra of Silica Glass," *PRL* **106**, 027401 (2011).
15. J. Bude, G. Guss, M. Matthews, and M. L. Spaeth, "The effect of lattice temperature on surface damage in fused silica optics," *Proceedings of the SPIE - The International Society for Optical Engineering* **6720**, 672009 (2007).

16. N. Shen, J. Bude, and C. W. Carr, "Model laser damage precursors for high quality optical materials," *Optics Express*, in press (2014).
17. J. Honig, M. Norton, W. Hollingsworth, E. Donohue, M. Johnson, "Experimental study of 351-nm and 527-nm laser initiated surface damage on fused silica surfaces due to typical contaminants," *SPIE*, Vol.. 5647, p. 129-135, (2005).
18. P. E. Miller, T. I. Suratwala, J. D. Bude, N. Shen, W. A. Steele, T. A. Laurence, M. D. Feit, and L. L. Wong, "Methods for globally treating silica optics to reduce optical damage," US8313662 (2012).
19. P. E. Miller, J. D. Bude, T. I. Suratwala, N. Shen, T. A. Laurence, W. A. Steele, J. Menapace, M. D. Feit, and L. L. Wong, "Fracture-induced subbandgap absorption as a precursor to optical damage on fused silica surfaces," *Optics Letters* **35**, 2702-2704 (2010).
20. T. A. Laurence, J. D. Bude, N. Shen, T. Feldman, P. E. Miller, W. A. Steele, and T. Suratwala, "Metallic-like photoluminescence and absorption in fused silica surface flaws," *Applied Physics Letters* **94**, 151114 (2009).
21. N. Shen et al, in preparation.
22. J. Adams M. Bolourchi, J. Bude, et al, "Results of applying a non-evaporative mitigation technique to laser-initiated surface damage on fused silica optics," *SPIE* vol. 7842, 784223 (2010).
23. R. M. Brusasco, B. M. Penetrante, J. A. Butler, S. M. Maricle, and J. E. Peterson, "CO<sub>2</sub>-laser polishing for reduction of 351-nm surface damage initiation in fused silica," in *Laser-Induced Damage in Optical Materials: 2001 Proceedings*, G. Exarhos, A. H. Guenther, K. L. Lewis, M. J. Soileau, and C. J. Stolz, eds. (2002), pp. 34-39.
24. Baxamusa et al, submitted for publication.